


Article

# Corrosion Resistance of Mild Steel Coated with Orgainc Material Containing Pyrazol Moiety

Fadoua El Hajjaji <sup>1</sup>, Farid Abrigach <sup>2</sup>, Othman Hamed <sup>3,\*</sup>, Abdelfatah Rasem Hasan <sup>4</sup>, Mustapha Taleb <sup>1</sup>, Shehdeh Jodeh <sup>3,\*</sup> , Enrique Rodríguez-Castellón <sup>5</sup> , María del Valle Martínez de Yuso <sup>6</sup> and Manuel Algarra <sup>5,7</sup> 

<sup>1</sup> Laboratory of Engineering, Electrochemistry, Modeling and Environment, Faculty of Sciences, University sidi Mohamed Ben Abdellah, FEH Fez, Morocco; el.hajjajifadoua25@gmail.com (F.E.H.); mustaphataleb62@yahoo.fr (M.T.)

<sup>2</sup> LCAE-URAC 18, Faculty of Science, First Mohammed University, P.O. Box 717, 60000 Oujda, Morocco; abrigach.farid@live.fr

<sup>3</sup> Department of Chemistry, An-Najah National University, P.O. Box 7, Nablus WP, Palestine

<sup>4</sup> Water and Environmental Studies Institute, An-Najah National University, P.O. Box 7, Nablus WP, Palestine; mallah@najah.edu

<sup>5</sup> Departament of Inorganic Chemistry, Faculty of Sciences, University of Málaga, Campus de Teatinos s/n, 29071 Málaga, Spain; castellon@uma.es (E.R.-C.); malgarra67@gmail.com (M.A.)

<sup>6</sup> X-ray Photoelectron Spectroscopy Lab., Central Service to Support Research Building (SCAI), University of Málaga, 29071 Málaga, Spain; mvyuso@uma.es

<sup>7</sup> CQM—Centro de Química da Madeira, Universidade da Madeira, Campus da Penteada, 9020-105 Funchal, Portugal

\* Correspondence: ohamed@najah.edu (O.H.); sjodeh@hotmail.com (S.J.)

Received: 29 May 2018; Accepted: 24 August 2018; Published: 21 September 2018



**Abstract:** Pyridine (P1) and benzoic acid (P2) derivatives with pyrazole moieties were synthesized and evaluated as corrosion inhibitors for mild steel in acidic medium. The evaluation was performed by electrochemical impedance spectroscopy (EIS), potentiodynamic polarization, and weight loss measurement. The surface morphologies of the control and steel samples coated with the pyrazole derivatives P1 and P2 were examined by the scanning electron microscopy (SEM), UV-Vis, and X-ray photoelectron spectroscopy (XPS) spectroscopies. Results revealed minor changes on steel surfaces before and after immersion in a 1 M HCl solution. Both derivatives, P1 and P2, showed good inhibition efficiency that is dependent on inhibitor concentration. Both P1 and P2 act as mixed-type inhibitors. The benzoic acid derivative (P2) showed a higher efficiency than P1, which could be attributed to the carboxyl group that is located at the para position to the amino group. This induces a direct electronic resonance between the two groups, the amino and the carboxyl. As a result of this, a higher electron density on the carboxyl group and a stronger bonding to the metal surface occurred. Results also show that, the bonding of both pyrazoles on mild steel surface obey Langmuir adsorption isotherm. Quantum chemical calculations were performed to theoretically define the relationship between the molecular structures and inhibition efficiencies of P1 and P2.

**Keywords:** pyrazole; mild steel; corrosion resistance; potentiodynamic polarization; XPS spectroscopy

## 1. Introduction

Pickling process of steel includes using a strong acid such as hydrochloric acid or a mixture of hydrochloric acid and nitric acid. Residual acid on steel surface after the pickling process causes the steel to corrode. One way of overcoming this major issue is the use of an inhibitor [1–5]. Most of inhibitors used for this purpose are organic based materials contain coordination sites for

metal coordination. The coordination sites include multiple bonds and heteroatoms such as sulfur, oxygen and nitrogen. These inhibitors prevent corrosion by blocking the active corrosion sites mainly by complexing to the metal surface and forming a protective layer [6–8]. A strong interaction between the metal surface and the protective layer leads to a more stable and less protective layer. The strength of the interaction is usually controlled by the high electron density and the availability of the loose  $\pi$ -electrons on the inhibitors functional groups [9,10].

Unfortunately, most of the reported inhibitors are either toxic or have an environmental concern. For this reason, an inhibitor that is free of these drawbacks will be very attractive. One choice would be pyrazole based material. Pyrazole and pyrazole derivatives have the functionalities that require a strong interaction with the metal surface and are well known in the medical field. They are widely used as antimicrobials agents [11,12], antifungal agents [13,14], anti-inflammatory agents [15,16], anticancer agents [17,18] antitubercular agents [19,20].

Pyridine-pyrazoles are especially more useful for this purpose than other pyrazole derivatives since they have multi coordination sites which make them bind stronger to the metal surface. A study, on using pyridine-pyrazole derivatives as corrosion inhibitors, revealed a good anticorrosive efficiency. The presence of a side chain on pyrazole showed an increase in the efficiency of the pyrazole and the longer the chain the higher the higher efficiency [21]. Several pyrazole derivatives were evaluated as steel corrosion inhibitors in our laboratory [22–26].

In this work, two new pyrazole derivatives were synthesized and evaluated as corrosion inhibitors for steel in acidic media. The two pyrazole derivatives are pyridine and benzoic acid-based compounds. The pyridine based compound is *N*-((3,5-dimethyl-1*H*-pyrazol-1-yl) methyl)pyridine-4-amine (P1) and the benzoic acid based compound is 4-(((3,5-dimethyl-1*H*-pyrazol-1-yl)methyl)amino)benzoic acid (P2). The chemical structures of both compounds P1 and P2 are shown in Figure 1. Specimens of mild steels were coated with both materials and the anticorrosion properties of the coated steel were evaluated in a 1 M aqueous solution of HCl. The results were evaluated by several spectroscopic and gravimetric techniques such, electrochemical impedance spectroscopy, polarization measurements, Quantum chemical study, scanning electron microscopy (SEM), UV-Vis and XPS (X-ray photoelectron spectroscopy) spectroscopies.

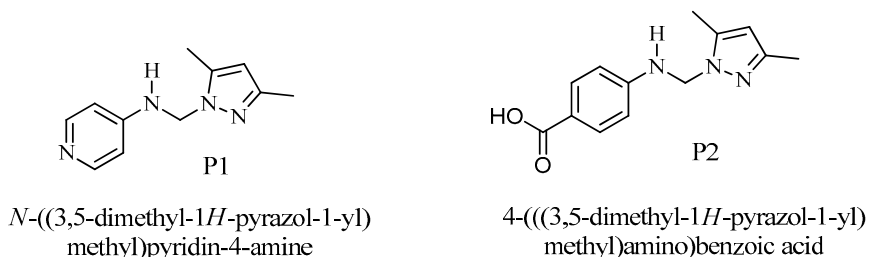


**Figure 1.** Chemical structures of the studied pyrazole derivatives pyridine (P1) and benzoic acid (P2).

## 2. Experimental

### 2.1. Materials

Specimens of mild steel were cut from a commercially available sheet of mild steel. The steel sheet composed of (in wt.%) 0.09 wt.% P, 0.01 wt.% Al, 0.38 wt.% Si, 0.05 wt.% Mn, 0.21 wt.% C, 0.05 wt.% S and the the remainder was iron (Fe). The exposed surface of the working electrodes was cleaned successively with emery papers of different grade (220, 400, 800, 1000 and 1200), washed with deionized water, acetone, ultrasonically cleaned with ethanol and stored in moisture free desiccator before it was used. The two studied pyrazoles P1 and P2 were synthesized as described in the literature [27].

## 2.2. Solutions

An aqueous solution of HCl (1 M) was prepared from concentrated HCl (37%, analytical grade) by dilution with Milli Q water. Solutions of *N*-((3,5-dimethyl-1*H*-pyrazol-1-yl)methyl)pyridin-4-amine (P1) and 4-(((3,5-dimethyl-1*H*-pyrazol-1-yl)methyl)amino)benzoic acid (P2) solutions were prepared in water with various concentrations.

## 2.3. Methods

### 2.3.1. Gravimetric Analysis

Gravimetric analysis was performed following the guidance of the ASTM method G31-72 [28]. Sheets of mild steel with dimensions of  $S = 10 \text{ mm} \times 40 \text{ mm} \times 0.6 \text{ mm}$  were scraped with a series of emery paper SIC (220, 400, 800, 1000 and 1200), washed with doubly distilled water then acetone. After weighing them accurately on an analytical balance, the specimens were immersed in a 250-mL beaker containing 100 mL of HCl (1 M) solution with and without the addition of inhibitors solutions. All solutions were kept under an ambient condition. After 6 h of immersion in an acid solution, the steel samples were removed, washed with plenty of distilled water, dried, and weighed. All tests were carried out in triplicate and the average results were reported. Relative errors are shown on the table. The loss in the weight ( $w$ ), The inhibition efficiency ( $IE$ ) and surface coverage ( $\theta$ ) of coated samples were calculated according to Equations (1)–(3) [28]:

$$w = \frac{w_a - w_b}{St} \quad (1)$$

$$IE(\%) = \left(1 - \frac{w_i}{w_0}\right) \times 100 \quad (2)$$

$$\theta = 1 - \frac{w_i}{w_0} \quad (3)$$

where  $w_b$  and  $w_a$  are the specimen weights before and after immersion in the acid solutions,  $w_0$  and  $w_i$  are the loss in the weight due to corrosion of steel samples in uninhibited and inhibited solutions, respectively. The total area of the mild steel specimen ( $\text{cm}^2$ ) represented as  $S$  and  $t$  are immersion time (h) as shown in Equation (1).

### 2.3.2. Electrochemical Evaluation

The electrochemical evaluation was performed using Voltalab (Tacussel-Radiometer PGZ 100, Hatch Company, Mississauga, ON, Canada) potentiostat that is run by Tacussel corrosion analysis software model (Voltamaster4) at static conditions. Electrochemical cell with three electrodes was used in this study; the reference electrode (a saturated calomel electrode (SCE)), an auxiliary electrode (platinum electrode with a surface area of  $1.0 \text{ cm}^2$ ) and the working electrode which is mild steel of surface area of  $1.0 \text{ cm}^2$ . All potential values used in this study were referred to this reference electrode. The mild steel electrode (working electrode) was dipped in a test solution for 30 min to establish a steady state open circuit potential ( $E_{\text{ocp}}$ ). After determining the value of the  $E_{\text{ocp}}$ , the electrochemical measurements were carried out. All electrochemical measurements were carried out in aerated solutions at 308 K. The electrochemical impedance spectroscopy (EIS) experiments were conducted at a frequency range of 10 mHz–100 KHz, with 10 points per decade at the rest potential, after 30 min of acid immersion and applying 10 mV ac voltage peak-to-peak. Nyquist plots were performed on experimental results. The accepted semicircle is the one that could be fit through the data points in the Nyquist plot using a non-linear least square fit, so as it intercepts with the  $x$ -axis. The impedance data were analyzed and fitted with the simulation  $Z_{\text{view}}$  2.80, equivalent circuit software. The potentiodynamic polarization measurements of mild steel samples in inhibited and uninhibited solutions were scanned from cathodic to the anodic direction, with a scan rate of  $0.5 \text{ mV/s}$ .

Data analysis was carried out using the polarization VoltaMaster 4 software. The linear Tafel segments of anodic and cathodic curves were extrapolated to corrosion potential to obtain corrosion current densities ( $I_{\text{corr}}$ ). From the obtained polarization curves, the cathodic reaction is dominated by hydrogen evolution as compared to  $\text{O}_2$  reduction consequently the corrosion current ( $I_{\text{corr}}$ ) was calculated according to Tafel extrapolation using Equation (4) [29]:

$$I = I_{\text{corr}} \left[ \exp\left(\frac{2.3\Delta E}{\beta_a}\right) - \exp\left(\frac{2.3\Delta E}{\beta_c}\right) \right] \quad (4)$$

The inhibition efficiency was evaluated using measured  $I_{\text{corr}}$  values as shown in Equation (5) [29]:

$$IE(\%) = \frac{I_{\text{corr}} - I_{\text{corr}(i)}}{I_{\text{corr}}} \times 100 \quad (5)$$

The  $I_{\text{corr}}$  is the corrosion current density for steel electrode in the uninhibited and the  $I_{\text{corr}(i)}$  is for the pyrazol solution.

## 2.4. Surface Morphology Evaluation

### 2.4.1. Scanning Electron Microscopy (SEM)

The SEM study was carried out on mild steel samples treated with 1.0 M solution of HCl containing P1 and P2 at concentration of  $10^{-3}$  M for 24 h. The samples before placed in the SEM were rinsed with double distilled water and dried with cold air blower. Similar SEM study was also performed on steel samples immersed in uninhibited HCl solution.

The scanning electron study was carried out using SEM model Quanta 200 FEI scanning instrument (Thermo Fisher Scientific, Waltham, MA, USA) at an accelerating voltage of 20 kV and 2000 $\times$  magnification.

### 2.4.2. UV-Visible

The UV-Visible absorption spectra of solutions containing optimum concentration ( $10^{-3}$  M) of inhibitor before and after immersion of the mild steel sample for 24 h were subjected to UV analysis using the Shimadzu model UV-1650 PC spectrophotometer (Shimadzu, Kyoto, Japan).

### 2.4.3. XPS Analysis

The surface has been analyzed by XPS to determine its composition. XPS studies were acquired on a Physical Electronics PHI VersaProbe II spectrometer (Chanhassen, MN, USA) using monochromatic Al-K $\alpha$  radiation (49.1 W, 15 kV, and 1486.6 eV) for analyzing the core-level signals of the elements of interest with a hemispherical multichannel detector. The sample spectra were recorded with a constant pass energy value at 29.35 eV, using a 200  $\mu\text{m}$  diameter circular analysis area. The X-ray photoelectron spectra obtained were analyzed using PHI SmartSoft software and processed using MultiPak 9.3 package. The binding energy values were referenced to adventitious carbon C 1s signal (284.8 eV). Shirley-type background and Gauss-Lorentz curves were used to determine the binding energies. XPS spectroscopy studies the adsorption of the pyrazole on steel surface and indicates the inhibition film. The analysis of the C 1s core level signals was very useful in identifying the different functional groups at the surface, such as their adsorption on surface.

## 2.5. Quantum Chemical Calculations

Geometrical optimization of the investigated samples was performed using density functional theory (DFT), using the Lee-Yang-Parr nonlocal correlation functional (B3LYP), and the Beck's three parameters exchange functional [29–31]. The 6-31G\* basis set was applied in the Gaussian 03 program package [32]. The adopted approach is shown to produce favorable geometries for a wide variety

of systems. This basis set produces good geometry optimizations. The geometry structure was optimized under no constraint. The quantum chemical parameters the highest occupied molecular orbital ( $E_{\text{HOMO}}$ ), the lowest unoccupied molecular orbital ( $E_{\text{LUMO}}$ ), the energy gap ( $\Delta E$ ) and the dipole moment ( $\mu$ ) were calculated from the optimized structure.

### 3. Results and Discussion

#### 3.1. Gravimetric Analysis

##### 3.1.1. Effect of Pyrazols Concentration

The corrosion rate ( $w$ ) and the  $IE$  (%) value obtained from gravimetric analysis method at various concentrations of P1 and P2 are shown in Table 1.

**Table 1.** Weight loss data for mild steel in 1.0 M HCl without and with different concentrations of pyrazole derivatives at 308 K.

Inhibitor	Conc. (M)	$w$ (mg cm <sup>-2</sup> h <sup>-1</sup> )	$IE$ (%) $\pm$ 1%	$\theta$
P1	$1 \times 10^{-3}$	0.081	89.5	0.895
	$5 \times 10^{-4}$	0.125	87.0	0.870
	$1 \times 10^{-4}$	0.158	83.3	0.833
	$5 \times 10^{-5}$	0.160	83.6	0.836
P2	$1 \times 10^{-3}$	0.058	94.0	0.940
	$5 \times 10^{-4}$	0.082	91.4	0.914
	$1 \times 10^{-4}$	0.147	84.0	0.840
	$5 \times 10^{-5}$	0.175	81.8	0.818

The results show that compounds P1 and P2 inhibit the corrosion of mild steel at all evaluated concentrations. The corrosion inhibition of these compounds could be related to the non-bonding electrons on the heteroatoms (N and O) and the aromatic  $\pi$  electrons, which causes a strong coordination of the inhibitors to the metal surface and the formation of a stable protective layer [33]. The corrosion rates in the presence of P1 and P2 were 0.081 and 0.058 mg cm<sup>-2</sup> h<sup>-1</sup>, respectively (Table 1). These values are much lower than that for the blank which is 0.962 mg cm<sup>-2</sup> h<sup>-1</sup>. This significant reduction in the corrosion rate suggests that the pyrazole derivatives are very effective as corrosion inhibitors even in solution with high acid concentration.

##### 3.1.2. Adsorption Isotherm and Standard Adsorption Free Energy

The types of interaction that occur between an organic inhibitor and a surface of mild steel could be calculated from studying the adsorption isotherms. The most useful adsorption isotherms are Langmuir, Temkin, and Frumkin. The surface coverage ( $\theta$ ) for various concentrations of P1 and P2 in HCl (1 M) were tested graphically to determine a suitable adsorption isotherm.

Figure 2 shows a graph obtained from plotting  $C/\theta$  versus  $C$ —a linear relationship was obtained, with a correlation coefficient ( $R^2$ ) values of 0.99973 and 0.99981 for P1 and P2, respectively, at 308 K. The results indicate that the adsorption of the inhibitors P1 and P2 on the metal surface could be fitted to the Langmuir adsorption isotherm shown in Equation (6) [33].

$$\frac{C}{\theta} = \frac{1}{K_{\text{ads}}} + C \quad (6)$$

where  $\theta$  is the surface coverage obtained from Equation (3),  $K_{\text{ads}}$  is the adsorption-desorption equilibrium constant,  $C$  is the concentration of inhibitor.

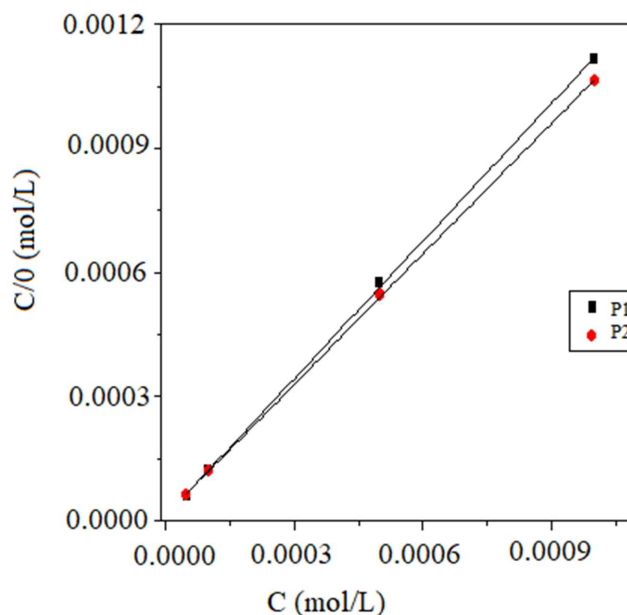


**Figure 2.** Langmuir adsorption isotherms for P1 and P2 on mild steel in 1.0 M HCl at 308 K.

The values of  $K_{\text{ads}}$  were calculated from the intercepts in Figure 2, the results are summarized in Table 2. As shown in Table 2, the results indicate a stable protective layer of P1 and P2 on the metal surface and hence good anticorrosion properties. The calculated values of  $K_{\text{ads}}$  were used in Equation (7) to obtain the  $\Delta G_{\text{ads}}^0$  values [34].

$$\Delta G_{\text{ads}}^0 = -RT \ln(55.5 K_{\text{ads}}) \quad (7)$$

where  $R$  is the gas constant,  $T$  is the temperature in K, and the 55.5 value represents the concentration of water in the solution. Obtained values of  $\Delta G_{\text{ads}}^0$  are shown in Table 2.

**Table 2.** Thermodynamic parameters for the adsorption of P1 and P2 in 1 M HCl on the mild steel at 308 K.

Inhibitors	Slopes	$K_{\text{ads}}$ ( $\text{M}^{-1}$ )	$R^2$	$\Delta G_{\text{ads}}^0$ (kJ/mol)
P1	1.11	111884.23	0.99973	−40.05
P2	1.05	77893.75	0.99981	−39.13

The negative values of  $\Delta G_{\text{ads}}^0$  suggest the spontaneous process of adsorption besides the stability of the thin layer adsorbed on the mild steel surface.

Literature demonstrates that, the standard Gibbs free energy of adsorption in aqueous solution with a value up to  $-20 \text{ kJ mol}^{-1}$  or more positive indicates electrostatic attraction taking place between the charged inhibitor molecules and metal surface (physisorption). While if this value is close to  $-40 \text{ kJ mol}^{-1}$  or more negative, the adsorption involves sharing or transfer of charges to the surface (chemisorption) [34]. However, this conclusion should be considered with some caution, since the enthalpy of adsorption is the parameter that reflects the adsorption bond strength, rather than the standard Gibbs free energy of adsorption [35]. In the present study,  $\Delta G_{\text{ads}}^0$  values are between  $-39.13$  and  $-40.05 \text{ kJ/mol}$ . These values provide evidence for the presence of chemisorption [36].

### 3.2. Potentiodynamic Polarization Curves

The potentiodynamic measurement results of mild steel in an aqueous solution of HCl (1.0 M) without and with P1 and P2 at different concentrations are shown in Figure 3.



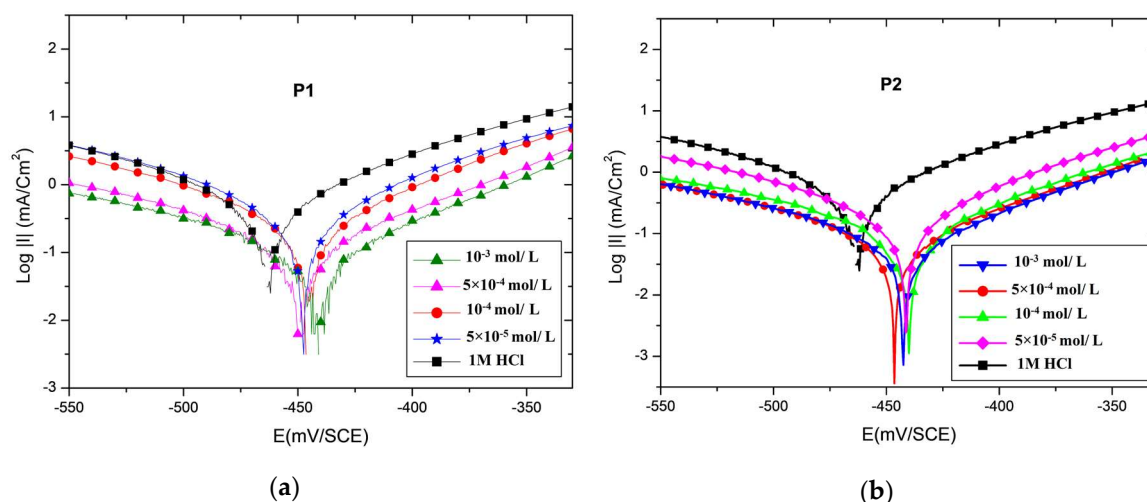


**Figure 3.** Polarization curves for mild steel in 1.0 M HCl in the presence and absence of various concentrations of (A) P1 and (B) P2.

The polarization parameters corrosion current density ( $I_{\text{corr}}$ ), anodic Tafel slope ( $\beta_a$ ), corrosion potential ( $E_{\text{corr}}$ ) cathodic Tafel slope ( $\beta_c$ ) and percentage inhibition efficiency  $IE$  (%) were all calculated from the Tafel curves shown in Table 3. The results show that both the cathodic and anodic reactions were suppressed in the presence of P1 and P2 inhibitors. Because of this, the pyrazole derivatives tend to reduce the anodic dissolution and reactions results in the evolution of hydrogen [37].

**Table 3.** The electrochemical parameters for mild steel in 1.0 M HCl solution without and with various concentrations of pyrazole derivatives at 308 K.

Medium	Conc (M)	$-E_{\text{corr}}$ (mV <sub>SCE</sub> )	$-\beta_a$ (mV dec <sup>-1</sup> )	$-\beta_c$ (mV dec <sup>-1</sup> )	$I_{\text{corr}}$ ( $\mu\text{A cm}^{-2}$ )	$IE$ (%)
HCl	1	450	105	207	1870.0	—
P1	$1 \times 10^{-3}$	442	78	165	115.2	93
	$5 \times 10^{-4}$	450	99	180	338.3	82
	$1 \times 10^{-4}$	449	95	140	455.2	75
	$5 \times 10^{-5}$	447	96	150	529.3	71
P2	$1 \times 10^{-3}$	442	79	145	66.5	96
	$5 \times 10^{-4}$	446	79	135	125.0	93
	$1 \times 10^{-4}$	439	85	165	187.8	90
	$5 \times 10^{-5}$	441	92	172	253.0	86

As shown in Figure 3, it could be concluded that the corrosion potentials ( $E_{\text{corr}}$ ) for the mild steel in the presence of P1 (Figure 3A) and P2 (Figure 3B) are slightly shifted toward a positive potential compared to the mild steel in the blank solution. Both anodic and cathodic current densities were reduced in the presence of P1 and P2, which suggests a mixed-type of inhibition with the predominance of anodic [38]. The Tafel slopes of the anodic ( $\beta_a$ ) and the cathodic ( $\beta_c$ ) of P1 and P2 are proportional with the inhibitor concentration.

The results in Table 3 show that the inhibition efficiency is directly proportional with the concentration of the inhibitors, while the corrosion current density decreases due to adsorption of P1 and P2 on the surface of the mild steel [39]. A corrosion inhibition efficiency of 96% and 93% at a concentration of  $10^{-3}$  M were obtained for P1 and P2, respectively.

### 3.3. Electrochemical Impedance Spectroscopy (EIS)

The degree of the corrosion protection could be determined by comparing the impedance values obtained in the presence and absence of an inhibitor in a corrosive environment. The Nyquist plots for

mild steel obtained in an aqueous solution of HCl (1 M) interface with and without P1 and P2 at 308 K are shown in Figure 4 respectively.

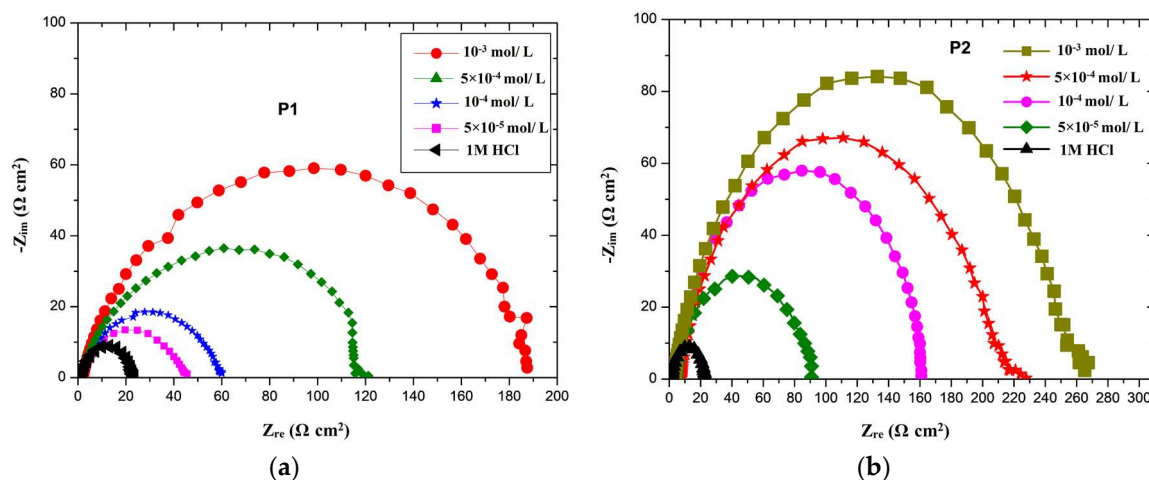


**Figure 4.** Impedance diagrams of (a) P1 and (b) P2 at  $10^{-3}$  M concentration for mild steel in 1 M HCl solution at 308 K.

The Nyquist plots are shown in Figure 4 exhibits depressed capacitive loop, which could be related to the charge transfer reaction. The depression in semicircle loop is usually related to the inhomogeneities and the roughness of the solid electrode [40]. As shown in Figure 4, the diameter of the capacitive loop increases by increasing the concentration of the pyrazoles.

This result indicates that corrosion is prevented by the formation of a protective film on the surface of the mild steel. The impedance kinetic parameters were determined by fitting the impedance data to the equivalent circuit model of the form  $R_s(R_{ct} \text{ CPE})$  as shown in Figure 5. The excellent fit was obtained with this model for all the experimental data.

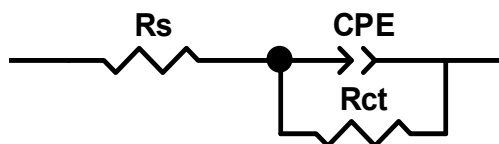


**Figure 5.** Equivalent circuit model used to fit the EIS data.

For the description of a frequency-independent phase shift between an applied ac potential and its current response, a constant phase element (CPE) was used, which is defined in impedance representation as [41]:

$$Z_{\text{CPE}} = \frac{1}{A(i\omega)^n} \quad (8)$$

where  $A$  ( $\Omega^{-1} \text{ s}^n \text{ cm}^{-2}$ ) is the value of the CPE,  $\omega$  (rad/s) is the sin wave modulation angular frequency,  $i^2 = -1$  is the imaginary number and  $n$  is an empirical exponent that measures the deviation from the ideal capacitive behavior [42,43]. Based on the values of  $n$ , CPE could be resistance for  $n = 0$ , capacitance for  $n = 1$ , or inductance for  $n = -1$  and  $n = 0.5$  for Warburg impedance [44–48]. The double layer capacitance ( $C_{dl}$ ) values can be calculated as shown in Equation (9) using  $n$  and CPE values [49]:

$$C_{dl} = \sqrt[n]{A(R_{ct})^{1-n}} \quad (9)$$

The impedance value on the real axis at high-frequency region corresponds to the solution resistance ( $R_s$ ), while the value at low-frequency region corresponds to the charge transfer



resistance ( $R_{ct}$ ). The  $R_{ct}$  values for the inhibited systems are higher than that of the blank and increases by increasing the concentration of the inhibitors. The results indicate that the studied pyrazole derivatives inhibit mild steel corrosion in HCl (1 M). The inhibition efficiency increases as the concentration of the inhibitors increases. The inhibition efficiency ( $IE$ ) was calculated from charge transfer resistance values obtained from impedance measurements using Equation (10) [49]:

$$IE (\%) = \frac{R_{ct/inh} - R_{ct}}{R_{ct/inh}} \times 100 \quad (10)$$

where  $R_{ct}$  and  $R_{ct/inh}$  are the charge transfer resistance of mild steel electrode in the uninhibited and inhibited solutions, respectively.

The values of phase shift  $n$  (ranging from 0.74 to 0.80) did not change significantly and its stability indicate that the charge transfer controlled the dissolution mechanism of mild steel in an aqueous solution of HCl (1 M) with inhibitor and for standard [50]. The relaxation time of a surface state is the time required the charge distribution to return to the equilibrium point after an electrical disturbance, in the absence of the distributed element. The relaxation time is defined as shown in Equation (11) [50]:

$$\tau = C_{dl}R_{ct} \quad (11)$$

The electrochemical kinetic parameters obtained from the fitting of impedance spectra are listed in Table 4.

**Table 4.** Impedance parameters with corresponding to inhibition efficiency for the corrosion of mild steel in 1.0 M HCl at different concentrations of pyrazole derivatives.

	Medium	$R_s (\Omega \text{ cm}^2)$	$n$	$R_{ct}/\text{Fit} (\Omega \text{ cm}^2)$	$R_{ct}/\text{Exp} (\Omega \text{ cm}^2)$	$C_{dl} (\mu\text{F cm}^{-2})$	$\tau (\text{ms})$	$IE (\%)$
	Blank	2.02	0.80	23.26	20.35	158.89	3.23	—
P1	$5 \times 10^{-5} \text{ M}$	2.00	0.74	45.1	60.20	121.23	7.30	66.2
	$1 \times 10^{-4} \text{ M}$	1.97	0.76	60	72.50	114.56	8.30	71.9
	$5 \times 10^{-4} \text{ M}$	1.45	0.74	120.8	117.60	75.33	8.86	82.7
	$1 \times 10^{-3} \text{ M}$	1.82	0.77	187.5	183.10	71.95	13.17	88.9
P2	$5 \times 10^{-5} \text{ M}$	2.50	0.77	90	76.48	87.55	6.70	73.4
	$1 \times 10^{-4} \text{ M}$	2.52	0.79	161	152.60	74.02	11.29	86.7
	$5 \times 10^{-4} \text{ M}$	2.61	0.78	225	173.30	70.90	12.29	88.3
	$1 \times 10^{-3} \text{ M}$	2.76	0.79	262	248.00	58.18	14.43	91.8

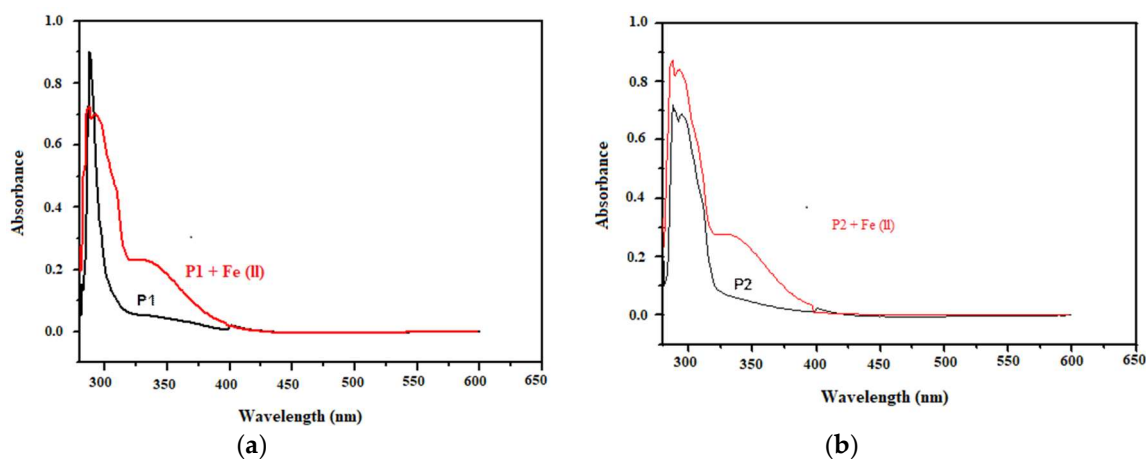
From Table 4, the inhibitors tend to decrease the double layer capacitance ( $C_{dl}$ ) and increase the time constant ( $\tau$ ) value. For instance, when the inhibitor concentration is increased to  $10^{-3} \text{ M}$ , the interface parameter ( $\tau$ ) changed from 3.23 to 14.43 ms while the double layer capacitance ( $C_{dl}$ ) value decreased from 158.89 to 58.18  $\mu\text{F cm}^{-2}$ . The results signify that the charge and discharge rate to the metal-solution interface is greatly decreased. This indicates that the presence of a relation between the amounts of charge that can be stored (i.e., capacitance) and the discharge velocity in the interface ( $\tau$ ) [51]. The double layer between the charged metal surface and the electrolyte solution is considered an electrical capacitor. The inhibitor molecules tend to eliminate the direct contact between  $\text{H}_2\text{O}$  molecules and the mild steel surface, and the electrical capacity consequently tends to decrease. As the concentration of the inhibitor increases, the electrical capacity concentrations—which could be attributed to the formation of a protective layer on the electrode surface [52]. The thickness of the protective layer is directly proportional with the inhibitor concentration. That means when the concentration of the inhibitor increases, the inhibitor molecules will be more electrostatically adsorbed on the electrode surface, then the double layer capacitance ( $C_{dl}$ ) decreases. This agrees with the Helmholtz model, shown in Equation (12) [53]:

$$C_{dl} = \frac{\epsilon_0 \epsilon}{d} S \quad (12)$$

where  $d$  and  $\varepsilon$  are the thickness and dielectric constant of the protective layer, respectively,  $\varepsilon_0$  is the permittivity of free space ( $8.854 \times 10^{-12} \text{ F m}^{-1}$ ) and  $S$  is the electrode surface area. As shown in Equation (12),  $C_{dl}$  is inversely proportional to the thickness of the protective layer ( $d$ ).

### 3.4. UV-Visible Spectroscopic Investigation of Inhibitor Solution

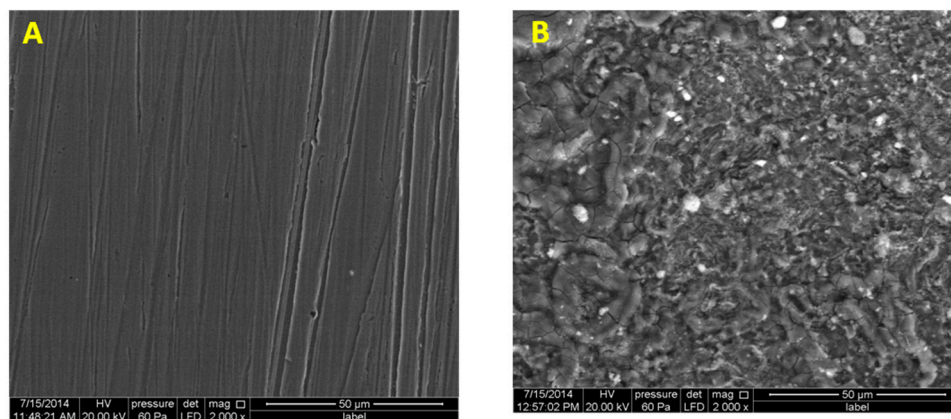
UV-Vis spectroscopic analysis was used to monitor compounds P1 and P2 in a 1.0 M solution of HCl (1 M) with inhibitors concentrations of  $10^{-3}$  M before and after immersion of mild steel. The obtained UV-Vis spectra for P1 and P2 spectra are presented in Figure 6, the spectra show a red shift and a decrease in the value of absorbance, the results suggest the formation of a complex between Fe(III)) and compounds P1 and P2 [54].



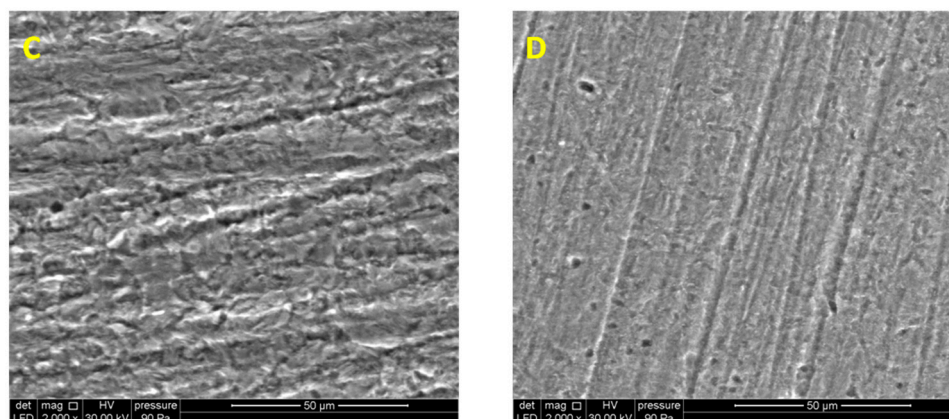
**Figure 6.** UV-Vis spectra of a 1.0 M HCl solution containing  $10^{-3}$  M of inhibitor before and after 24 h of mild steel immersion P1 (a) and P2 (b).

### 3.5. Scanning Electron Microscopy and XPS Analysis

The above results that indicate the effectiveness of the pyrazole derivatives as steel corrosion inhibitor by forming a protective film on steel surface were verified by the SEM micrographs. Which taken for mild steel surface after treatment with HCl (1 M) solution in the presence of pyrazoles ( $10^{-3}$  M) and for blank. The obtained images are shown in Figure 7.



**Figure 7.** Cont.



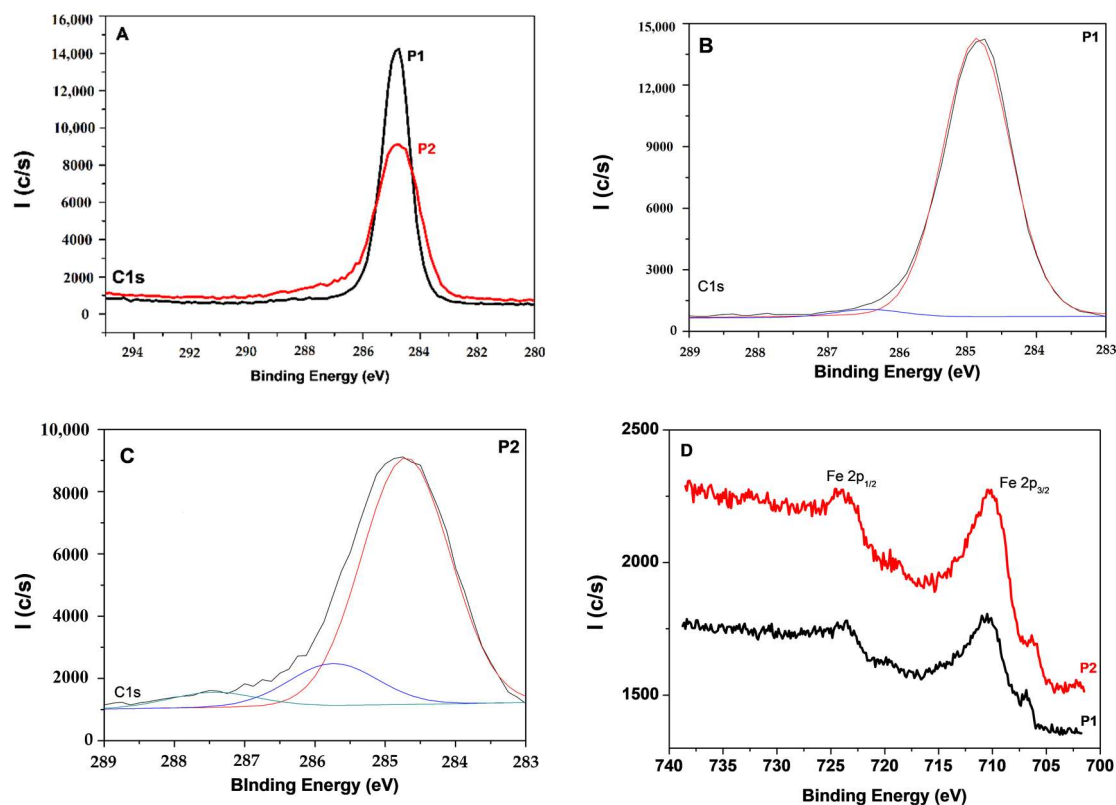
**Figure 7.** Scanning electron microscopy (SEM) images of mild steel surfaces; (A) abraded mild steel; (B) uninhibited treated with 1.0 M HCl; (C) P1; and (D) P2.

Figure 7A clearly shows the parallel features on the steel surface before exposure to the corrosive solution. The image of uninhibited steel surface is shown in Figure 7B. The image shows a rough surface, an indication of corrosion by HCl (1 M) solution. However, in the presence of pyrazole derivatives at a  $10^{-3}$  M concentration, the surface morphologies (Figure 7C,D) remarkably improved; the parallel features shown in Figure 7A can be clearly seen. The images clearly indicate that steel surface coated with P1 and P2 are protected against corrosion.

To confirm the presence of inhibitors on the steel surface, XPS analyses of the steel surfaces treated with P1 and P2 ( $10^{-3}$  M) in and immersed in a solution of HCl (1 M) for 2 h were carried out. Results are shown in Figure 8. A comparison between the C 1s core level spectra obtained for steel samples coated with P1 and P2 are shown in Figure 8A. The C 1s spectrum of sample treated with P2 shows a clear asymmetry in the high binding energy region. This could be due to the presence of the carboxylic group ( $-\text{COOH}$ ) in P2. The spectrum shown in Figure 8B belongs to steel sample coated with inhibitor P1 and it is deconvoluted in two contributions. The main contribution is broad and centred at 284.8 eV, and is assigned to  $-\text{CH}_3$  and  $-\text{C}=\text{C}-$  bonds of the inhibitor plus adventitious carbon. This contribution overlaps to that due to  $-\text{C}-\text{N}$  bonds. The second contribution is weak, and it is centred at 286.6 eV (5.0%) and assigned to  $\text{C}=\text{N}$  bonds of P1. The deconvoluted C 1s core level spectrum of the sample coated with P2 is shown in Figure 8C. This spectrum shows three contributions at 284.8 eV (75.1%), 286.1 eV (16.8%) and 288.1 eV (8.1%). The main contribution is due to  $-\text{C}=\text{C}-$  bonds and to adventitious carbon, while the contribution at 286.1 eV is assigned to  $-\text{C}-\text{N}-$  and  $-\text{C}=\text{N}-$  bonds. Finally, the third contribution at 288.1 eV is assigned to the presence of  $-\text{COOH}$  functional group [55]. Figure 8D shows the Fe 2p core level spectra (Fe  $2p_{3/2}$  at 710.9 eV), which identify the presence of Fe(III) on the surface, taken as reference  $\text{Fe}_2\text{O}_3$  [56], present as mentioned before a very low concentration (1.1%). These findings are verified by the Langmuir isotherm model obtained previously (Figure 2). The results indicate that both pyrazoles tend to stress corrosion process on steel surface. The Fe 2p spectra also show a weak peak at about 707.5 eV due to the subyacent Fe(0).

### 3.6. Quantum Chemical Calculations

In this study, quantum chemical calculations were performed to determine the relationship between the molecular structure of the P1 and P2 and their inhibition performance. The optimized molecular structures and the frontier molecule orbital density distribution of the studied molecules are shown in Figure 9, and the calculated quantum chemical indices  $E_{\text{HOMO}}$ ,  $E_{\text{LUMO}}$ ,  $\Delta E$ , and dipole moment ( $\mu$ ) are summarized in Table 5.



**Figure 8.** XPS C 1s core level spectra obtained for steel after treatment with HCl (1 M): (A) Comparison of the surface steel covered by P1 and P2 at  $10^{-3}$  M; (B) Deconvoluted C 1s spectrum of the surface steel covered by P1; (C) Deconvoluted C 1s spectrum of the surface steel covered by P2. (D) Fe 2p core level spectra of the surface steel covered by P1 and P2 at  $10^{-3}$  M.

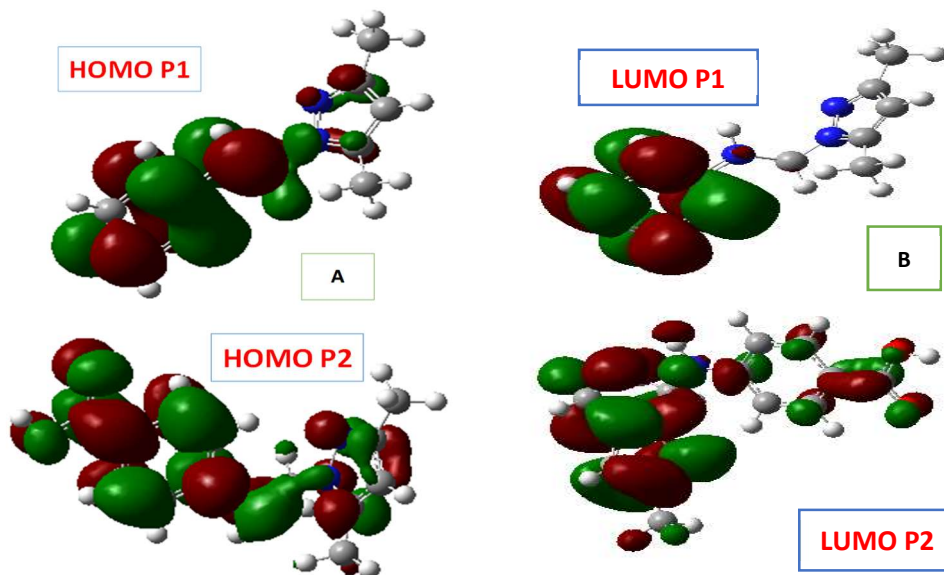


**Figure 9.** Optimized geometry and molecular orbital plots of studied pyrazole derivatives: (A) highest occupied molecular orbital (HOMO) and (B) lowest unoccupied molecular orbital (LUMO) for P1 and P2.

**Table 5.** Quantum chemical calculations parameters for P1 and P2.

Inhibitor	$E_{\text{HOMO}}$ (eV)	$E_{\text{LUMO}}$ (eV)	$\Delta E$ (eV)	$\mu$ (Debye)
P2	−8.54134	−4.39552	4.14582	3.6319
P1	−5.80012	−0.89434	4.90579	3.9252

Figure 9 shown that the highest occupied molecular orbital (HOMO) location in P1 is mostly distributed in the vicinity of over the entire molecule apart both methyl, however the distribution lowest unoccupied molecular orbital (LUMO) it is mainly localized on the pyridine ring. Whereas the HOMO and LUMO location in P2 are mostly distributed in the vicinity of the aminobenzoic acid, indicating that these are the binding sites to the metal surface adsorption. According to the frontier molecular orbital theory (FMO) of chemical reactivity, the transition of the electron is related to the interaction between HOMO and LUMO of reacting species [57].  $E_{\text{HOMO}}$  is a quantum chemical parameter which is often associated with the electron donating ability of the molecule. The high value of  $E_{\text{HOMO}}$  is likely to indicate a high tendency of a molecule to donate electrons to acceptor [58]. The inhibitor seems to donate an electron to the unoccupied d orbital of the metal ion and accept the electron from the d-orbital of the metal leading to back  $\pi$ -bonding. According to the obtained result, the highest  $E_{\text{HOMO}}$  value −5.80012 eV of P2 indicates a high inhibition efficiency.

The tendency for the formation of back  $\pi$ -bonding depends on the value of  $E_{\text{LUMO}}$ . Since the lower the value of  $E_{\text{LUMO}}$ , the easier the transfer of the electrons to the d orbital [59]. The values of  $E_{\text{LUMO}}$ , shows no correlation between the experimental results and theoretical calculations. Reportedly, excellent corrosion inhibitors are shown by organic compounds since it seems to donate electrons to the unoccupied orbital of the metal and accept electrons from the metal [60]. The energy gap, ( $\Delta E = E_{\text{LUMO}} - E_{\text{HOMO}}$ ) is an important parameter that influences the reactivity of the inhibitor molecule towards the metallic surface. As  $\Delta E$  decreases, the reactivity of the molecule increases leading to an increase in the  $IE\%$  of the molecule. Small energy difference will render good inhibition efficiency because the electronaffinity will be low [61]. A low energy gap means the molecule is more polarizable (soft) and hence high chemical activity and low kinetic stability [62].

Some authors showed that an increase of the dipole moment that it might cause a decrease in the inhibition and vice versa. So, lower values of the dipole moment will favor the accumulation of the inhibitor on the surface layer. In contrast, high dipole moment can lead to an increase in the inhibition and vice versa, which could be related to a dipole-dipole interaction of molecules and metal surface [63]. The higher value of  $\mu$  obtained for P2 is coherent with the second explanation.

#### 4. Conclusions

In the present study, two pyrazole derivatives *N*-((3,5-dimethyl-1*H*-pyrazole-1-yl)methyl)pyridine-4-amine (P1) and 4-(((3,5-dimethyl-1*H*-pyrazole-1-yl)methyl)amino)benzoic acid (P2) were synthesized and evaluated as corrosion inhibitors for steel. The two compounds were chosen because they are easily synthesized and have multi coordination sites for steel, represented by the lone pairs of the electron on oxygen and nitrogen in addition to the  $\pi$ -electrons on the aromatic rings. Both compounds showed good inhibition efficiency and act as mixed-type of inhibitors for mild steel in hydrochloric acid solution. Compound P2 showed higher inhibition efficiency than P1, and the inhibition efficiency increased by increasing the inhibitor concentration. The inhibition occurs through adsorption of the inhibitor on the mild steel surface. The adsorption of the inhibitors obeys a Langmuir adsorption isotherm. The high  $K_{\text{ads}}$  values indicate a strong interaction between the inhibitors and the carbon steel surface. The calculated  $\Delta G_{\text{ads}}^0$  values suggest the presence of chemisorption. The potentiodynamic polarization curves indicated that pyrazole derivatives are acting as mixed inhibitors with the predominance of the anodic. The EIS results revealed the formation of a protective film on the mild steel surface. UV-Vis spectroscopic studies revealed the occurrence of chemical interactions between the inhibitors and iron in the mild steel. SEM images and spectra obtained by XPS spectroscopy confirmed the



deposition of pyrazole derivatives on the mild steel surface. Quantum chemical studies support the experimental results.

**Author Contributions:** Methodology, M.T. and O.H.; Software, E.R.-C. and M.d.V.M.d.Y.; Validation, M.A.; Formal Analysis, S.J. and A.H.; Investigation, F.E.H. and F.A.; Data Curation, O.H. and A.H.; Writing—Original Draft Preparation, S.J. and M.T.; Writing—Review & Editing, S.J. and O.H.

**Funding:** This research received no external funding.

**Acknowledgments:** The authors would also like to thank An-Najah National University for providing the necessary equipments and lab for getting this work accomplished.

**Conflicts of Interest:** The authors declare no conflict of interest.

## References

1. Bedair, M.A. The effect of structure parameters on the corrosion inhibition effect of some heterocyclic nitrogen organic compound. *J. Mol. Liq.* **2016**, *219*, 128–141. [\[CrossRef\]](#)
2. El Faydy, M.; Galai, M.; El Assyry, A.; Tazouti, A.; Touir, R.; Lakhrissi, B.; EbnTouhami, M.; Zarrouk, A. Experimental investigation on the corrosion inhibition of carbon steel by 5-(chloromethyl)-8-quinolinol hydrochloride in hydrochloric acid solution. *J. Mol. Liq.* **2016**, *219*, 396–404. [\[CrossRef\]](#)
3. El-Hajjaji, F.; Messali, M.; Aljuhani, A.; Aouad, M.R.; Hammouti, B.; Belghiti, M.E.; Chauhan, D.S.; Quraishi, M.A. Pyridazinium-based ionic liquids as novel and green corrosion inhibitors of carbon steel in acid medium: Electrochemical and molecular dynamics simulation studies. *J. Mol. Liq.* **2018**, *249*, 997–1008. [\[CrossRef\]](#)
4. Ech-chihbi, E.; Belghiti, M.E.; Salima, R.; Oudda, H.; Taleb, M.; Benchat, N.; Hammouti, B.; El-Hajjaji, F. Experimental and computational studies on the inhibition performance of the organic compound “2-phenylimidazo [1,2-a]pyrimidine-3-carbaldehyde” against the corrosion of carbon steel in 1.0 M HCl solution. *Surf. Interfaces* **2017**, *9*, 206–217. [\[CrossRef\]](#)
5. Ghazoui, A.; Zarrouk, A.; Bencat, N.; Salghi, R.; Assouag, M.; el Hezzat, M.; Guenbour, A.; Hammouti, B. New possibility of mild steel corrosion inhibition by organic heterocyclic compound. *J. Chem. Pharm. Res.* **2014**, *6*, 704–712.
6. Bouoidina, A.; El-Hajjaji, F.; Drissi, M.; Taleb, M.; Hammouti, B.; Chung, I.L.; Jodeh, S.; Lgaz, A.H. Towards a deeper understanding of the anticorrosive properties of hydrazine derivatives in acid medium: experimental, DFT and MD simulation assessment. *Metall. Mater. Trans. A* **2018**, in press. [\[CrossRef\]](#)
7. El-Hajjaji, F.; Belghiti, M.E.; Hammouti, B.; Jodeh, S.; Hamed, O.; Lgaz, H.; Salghi, R. Adsorption and corrosion inhibition effect of 2-mercaptobenzimidazole (surfactant) on a carbon steel surface in an acidic medium: Experimental and monte carlo simulations. *Port. Electrochim. Acta* **2018**, *36*, 197–212. [\[CrossRef\]](#)
8. Hmamou, D.B.; Aouad, M.R.; Salghi, R.; Zarrouk, A.; Assouag, M.; Benali, O.; Messali, M.; Zarrouk, H.; Hammouti, B. Inhibition of C38 steel corrosion in hydrochloric acid solution by 4,5-Diphenyl-1H-Imidazole-2-Thiol: Gravimetric and temperature effects treatment. *J. Chem. Pharm. Res.* **2012**, *4*, 3498–3504.
9. Belayachi, M.; Serrar, H.; Zarrouk, H.; el Assyry, A.; Zarrouk, A.; Oudda, H.; Boukhris, S.; Hammouti, B.; Ebenso, E.E.; Geunbour, A. New pyrimidothiazine derivative as corrosion inhibitor for carbon steel in acidic media. *Int. J. Electrochem. Sci.* **2015**, *10*, 3010–3025.
10. Yadav, M.; Sinha, R.R.; Kumar, S.; Bahadur, I.; Ebenso, E.E. Synthesis and application of new acetohydrazide derivatives as a corrosion inhibition of mild steel in acidic medium: Insight from electrochemical and theoretical studies. *J. Mol. Liq.* **2016**, *208*, 322–332. [\[CrossRef\]](#)
11. Dabholkar, V.N.; Ansari, F.Y. Synthesis and characterization of selected fused isoxazole and pyrazole derivatives and their antimicrobial activity. *J. Serb. Chem. Soc.* **2009**, *74*, 1219–1228. [\[CrossRef\]](#)
12. Youssef, M.M.; Mohammed, S.F.; Kotb, E.R.; Salma, M.A. A novel synthesis of some new pyrimidine, thiazolopyrimidine and pyrazole derivatives using diarylepoxypyranones as precursor. *World J. Chem.* **2009**, *4*, 149–156.
13. Priyadarsini, P.; Ujwala, B.; Venkata Rao, C.; Madhava Rao, V. Synthesis and antimicrobial activity of some novel pyrazoles. *Pharm. Lett.* **2012**, *4*, 1123–1128.



14. Hassan, S.Y. Synthesis, Antibacterial and antifungal activity of some new pyrazoline and pyrazole derivatives. *Molecules* **2013**, *18*, 2683–2711. [[CrossRef](#)] [[PubMed](#)]
15. Jyoti, S.A.; Yadav, M.; Pathak, D. Synthesis and characterization of some substituted pyrazoles as analgesics and anti-inflammatory agents. *Pharm. Chem.* **2011**, *3*, 215–222.
16. Bhaskar, V.H.; Mohite, P.B. Design, synthesis, characterization and biological evaluation of some novel 1,5-disubstituted tetrazole as potential anti-inflammatory agent. *J. Optoelectron. Biomed. Mater.* **2010**, *2*, 231–237.
17. Al-Saadi, M.S.M. Synthesis and in vitro antitumour activity of some fused pyrazole and pyrazoline ring systems. *Saudi Pharm. J.* **2008**, *16*, 135–145.
18. Kalirajan, R.; Rathore, L.; Jubie, S.; Gowramma, B.; Gomathy, S.; Sankar, S.; Elango, K. Microwave assisted synthesis and biological evaluation of pyrazole derivatives of benzimidazoles. *Indian J. Pharm. Edu. Res.* **2010**, *44*, 358–362.
19. Kini, S.G.; Bhat, A.R.; Bryant, B.; Williamson, J.S.; Dayan, F.E. Synthesis, antitubercular activity and docking study of novel cyclic azole substituted diphenyl ether derivatives. *Eur. J. Med. Chem.* **2009**, *44*, 492–500. [[CrossRef](#)] [[PubMed](#)]
20. Babu, V.H.; Manna, S.K.; Srinivasson, K.K.; Bhatt, G.V. Synthesis and biological evaluation of 1,3,5-trisubstituted pyrazolines bearing benzofuran. *Indian J. Heterocycl. Chem.* **2004**, *13*, 253–256.
21. Driver, R.; Meakins, R.J. Contrasting behaviour of mild steel and pure iron towards pickling inhibitors. *Br. Corros. J.* **1977**, *12*, 46–50. [[CrossRef](#)]
22. Zarrok, H.; Oudda, H.; El Midaoui, A.; Zarrouk, A.; Hammouti, B.; Ebn Touhami, M.; Attayibat, A.; Radi, S.; Touzani, R. Some new bipyrazole derivatives as corrosion inhibitors for C38 steel in acidic medium. *Res. Chem. Intermed.* **2012**, *38*, 2051–2063. [[CrossRef](#)]
23. Tebbji, K.; Aouniti, A.; Attayibat, A.; Hammouti, B.; Oudda, H.; Benkaddour, M.; Radi, S.; Nahle, A. Inhibition efficiency of two bipyrazole derivatives on steel corrosion in hydrochloric acid media. *Indian J. Chem. Technol.* **2011**, *18*, 244–253.
24. Tebbji, K.; Oudda, H.; Hammouti, B.; Benkaddour, M.; Al-Deyab, S.S.; Aouniti, A.; Radi, S.; Ramdani, A. The effect of 1',3,5,5'-tetramethyl-1'H-1,3'-bipyrazole on the corrosion of steel in 1.0 M hydrochloric acid. *Res. Chem. Intermed.* **2011**, *37*, 985–1007. [[CrossRef](#)]
25. Benabdellah, M.; Touzani, R.; Aouniti, A.; Dafali, A.; el Kadiri, S.; Hammouti, B.; Benkaddour, M. Inhibitive action of some bipyrazolic compounds on the corrosion of steel in 1 M HCl: Part I: Electrochemical study. *Mater. Chem. Phys.* **2007**, *105*, 373–379. [[CrossRef](#)]
26. Elayyachy, M.; Elkodadi, M.; Aouniti, A.; Ramdani, A.; Hammouti, B.; Malek, F.; Elidrissi, A. New bipyrazole derivatives as corrosion inhibitors for steel in hydrochloric acid solutions. *Mater. Chem. Phys.* **2005**, *93*, 281–285. [[CrossRef](#)]
27. Abridgach, F.; Khoutoul, M.; Benchat, N.; Radi, S.; Draoui, N.; Feron, O.; Riant, O.; Touzani, R. Library of synthetic compounds based on pyrazole unit: Design and screening against breast and colorectal cancer. *Lett. Drug Des. Discov.* **2012**, *11*, 1010–1016. [[CrossRef](#)]
28. ASTM G31-72(2004) *Standard Practices for Laboratory Immersion Corrosion Testing of Metals*; ASTM: West Conshohocken, PA, USA, 1990.
29. Gupta, N.K.; Verma, C.; Quraishi, M.A.; Mukherjee, A.K. Schiff's bases derived from llysine and aromatic aldehydes as green corrosion inhibitors for mild steel: Experimental and theoretical studies. *J. Mol. Liq.* **2016**, *215*, 47–57. [[CrossRef](#)]
30. Becke, A.D. A new mixing of Hartree-Fock and local density-functional theories. *J. Chem. Phys.* **1993**, *98*, 1372–1377. [[CrossRef](#)]
31. Lee, C.; Yang, W.; Parr, R.G. Development of the Colle-Salvetti correlation-energy formula into a functional of the electron density. *Phys. Rev. B* **1988**, *37*, 785–789. [[CrossRef](#)]
32. Ju, H.; Kai, Z.P.; Li, Y. Aminic nitrogen-bearing polydentate Schiff base compounds as corrosion inhibitors for iron in acidic media: A quantum chemical calculation. *Corros. Sci.* **2008**, *50*, 865–871. [[CrossRef](#)]
33. Lgaz, H.; Salghi, R.; Jodeh, S.; Hammouti, B. Insights into corrosion inhibition behavior of three chalcone derivatives for mild steel in hydrochloric acid solution. *J. Mol. Liq.* **2017**, *225*, 271–280. [[CrossRef](#)]
34. Bilgic, S.; Sahin, M. The corrosion inhibition of austenitic chromium-nickel steel in H<sub>2</sub>SO<sub>4</sub> by 2-butyn-1-ol. *Mater. Chem. Phys.* **2001**, *70*, 290–295. [[CrossRef](#)]

35. Gharebaa, S.; Omanovic, S. Interaction of 12-aminododecanoic acid with a carbon steel surface: Towards the development of green corrosion inhibitors. *Corros. Sci.* **2010**, *52*, 2104–2113. [[CrossRef](#)]
36. Noor, E.A. Temperature effects on the corrosion inhibition of mild steel in acidic solutions by aqueous extract of fenugreek leaves. *Int. J. Electrochem. Sci.* **2007**, *2*, 996–1017.
37. Fouda, A.S.; Elewady, Y.A.; El-Aziz, H.K.A. Corrosion inhibition of carbon steel by cationic surfactants in 0.5 M HCl solution. *J. Chem. Sci. Technol.* **2012**, *1*, 45–53.
38. Li, X.; Deng, S.; Fu, H.; Mu, G. Inhibition effect of 6-benzylaminopurine on the corrosion of cold rolled steel in H<sub>2</sub>SO<sub>4</sub> solution. *Corros. Sci.* **2009**, *51*, 620–634. [[CrossRef](#)]
39. Amar, H.; Tounsi, A.; Makayssi, A.; Derja, A.; Benzakour, J.; Outzourhit, A. Corrosion inhibition of Armco iron by 2-mercaptobenzimidazole in sodium chloride 3% media. *Corros. Sci.* **2007**, *49*, 2936–2945. [[CrossRef](#)]
40. Scendo, M.; Uznanska, J. The effect of ionic liquids on the corrosion inhibition of copper in acidic chloride solutions. *Int. J. Corros.* **2011**, *2011*, 718626. [[CrossRef](#)]
41. Zheng, X.; Zhang, S.; Li, W.; Gong, M.; Yin, L. Experimental and theoretical studies of two imidazolium-based ionic liquids as inhibitors for mild steel in sulfuric acid solution. *Corros. Sci.* **2015**, *95*, 168–179. [[CrossRef](#)]
42. Lopez, D.A.; Simison, S.N.; de Sánchez, S.R. The influence of steel microstructure on CO<sub>2</sub> corrosion. EIS studies on the inhibition efficiency of benzimidazole. *Electrochim. Acta* **2003**, *48*, 845–854. [[CrossRef](#)]
43. Stoyanov, Z.B.; Grafov, B.M.; Savova-Stoyanova, B.S.; Elkin, V.V. “Electrochemical Impedance”, Moscow: Nauka, 1991, 336p. *Rus. J. Electrochem.* **1994**, *30*, 1075–1076.
44. Amin, M.A.; Khaled, K.F.; Mohsen, Q.; Arida, H.A. A study of the inhibition of iron corrosion in HCl solutions by some amino acids. *Corros. Sci.* **2010**, *52*, 1684–1695. [[CrossRef](#)]
45. Musa, A.Y.; Kadhum, A.A.H.; Mohamad, A.B.; Takriff, M.S. Experimental and theoretical study on the inhibition performance of triazole compounds for mild steel corrosion. *Corros. Sci.* **2010**, *52*, 3331–3340. [[CrossRef](#)]
46. Jacob, K.S.; Parameswaran, G. Corrosion inhibition of mild steel in hydrochloric acid solution by Schiff base furoin thiosemicarbazone. *Corros. Sci.* **2010**, *52*, 224–228. [[CrossRef](#)]
47. Labjar, N.; Lebrini, M.; Bentiss, F.; Chihib, N.; ElHajjaji, S.; Jama, C. Corrosion inhibition of carbon steel and antibacterial properties of aminotris-(methylenephosphonic) acid. *Mater. Chem. Phys.* **2010**, *119*, 330–336. [[CrossRef](#)]
48. Zheng, X.; Zhang, S.; Li, W.; Yin, L.; He, J.; Wua, J. Investigation of 1-butyl-3-methyl-1H-benzimidazolium iodide as inhibitor for mild steel in sulfuric acid solution. *Corros. Sci.* **2014**, *80*, 383–392. [[CrossRef](#)]
49. Mallaiya, K.; Subramaniam, R.; Srikandan, S.S.; Gowri, S.; Rajasekaran, R.; Selvaraj, A. Electrochemical characterization of the protective film formed by the unsymmetrical Schiff’s base on the mild steel surface in acid media. *Electrochim. Acta* **2011**, *56*, 3857–3863. [[CrossRef](#)]
50. Ozcan, M.; Karadag, F.; Dehri, I. Investigation of adsorption characteristics of methionine at mild steel/sulfuric acid interface: An experimental and theoretical study. *Colloids Surf. A* **2008**, *316*, 55–61. [[CrossRef](#)]
51. Musa, A.Y.; Jalgham, R.T.T.; Mohamad, A.B. Molecular dynamic and quantum chemical calculations for phthalazine derivatives as corrosion inhibitors of mild steel in 1 M HCl. *Corros. Sci.* **2012**, *56*, 176–183. [[CrossRef](#)]
52. Lebrini, M.; Lagreneé, M.; Vezin, H.; Traisnel, M.; Bentiss, F. Experimental and theoretical study for corrosion inhibition of mild steel in normal hydrochloric acid solution by some new macrocyclic polyether compounds. *Corros. Sci.* **2007**, *49*, 2254–2269. [[CrossRef](#)]
53. Helmholtz, H. Studies on electrical boundary layers. *Ann. Phys.* **1879**, *243*, 337–382. [[CrossRef](#)]
54. Sundaravel, K.; Suresh, E.; Palaniandavar, M. Iron(III) complexes of tridentate N3 ligands as models for catechol dioxygenases: Stereoelectronic effects of pyrazole coordination. *Inorg. Chim. Acta* **2010**, *363*, 2768–2777. [[CrossRef](#)]
55. Li, W.; Rodríguez-Castellón, E.; Bandoz, T.J. Photosensitivity of g-C<sub>3</sub>N<sub>4</sub>/S-doped carbon composites: Study of surface stability upon exposure to CO<sub>2</sub> and/or water at ambient light. *J. Mater. Chem. A* **2017**, *5*, 24880–24891. [[CrossRef](#)]
56. Yamashita, T.; Hayes, P. Analysis of XPS spectra of Fe<sup>2+</sup> and Fe<sup>3+</sup> ions in oxide materials. *Appl. Surf. Sci.* **2008**, *254*, 2441–2449. [[CrossRef](#)]

57. Musa, A.Y.; Kadhum, A.H.; Mohamad, A.B.; Rohoma, A.B.; Mesmari, H. Electrochemical and quantum chemical calculations on 4,4-dimethyloxazolidine-2-thione as inhibitor for mild steel corrosion in hydrochloric acid. *J. Mol. Struct.* **2010**, *969*, 233–237. [[CrossRef](#)]
58. Gece, G.; Bilgic, S. Quantum chemical study of some cyclic nitrogen compounds as corrosion inhibitors of steel in NaCl media. *Corros. Sci.* **2009**, *51*, 1876–1878. [[CrossRef](#)]
59. Wang, H.; Wang, X.; Wang, H.; Wang, L.; Liu, A. DFT study of new bipyrazole derivatives and their potential activity as corrosion inhibitors. *J. Mol. Model.* **2007**, *13*, 147–153. [[CrossRef](#)] [[PubMed](#)]
60. Obot, I.B.; Obi-Egbedi, N.O.; Umoren, S.A. Adsorption characteristics and corrosion inhibitive properties of clotrimazole for aluminium corrosion in hydrochloric acid. *Int. J. Electrochem. Sci.* **2009**, *4*, 863–877.
61. Breket, G.; Hur, E.; Ogretir, C. Quantum chemical studies on some imidazole derivatives as corrosion inhibitors for iron in acidic medium. *J. Mol. Struct. THEOCHEM* **2002**, *578*, 79–88. [[CrossRef](#)]
62. Fleming, I. *Frontier Orbitals and Organic Chemical Reactions*; John Wiley & Sons: Hoboken, NJ, UAS, 1976.
63. Herrag, L.; Hammouti, B.; Elkadiri, S.; Aouniti, A.; Jama, C.; Vezin, H.; Bentiss, F. Adsorption properties and inhibition of mild steel corrosion in hydrochloric solution by some newly synthesized diamine derivatives: Experimental and theoretical investigations. *Corros. Sci.* **2010**, *52*, 3042–3051. [[CrossRef](#)]



© 2018 by the authors. Licensee MDPI, Basel, Switzerland. This article is an open access article distributed under the terms and conditions of the Creative Commons Attribution (CC BY) license (<http://creativecommons.org/licenses/by/4.0/>).